Electronic Supplementary Information

Engineering low-coordination atoms on RhPt bimetallene for 12-electron ethanol electrooxidation

Bin Sun,[a] Wei Zhong,[a] Xuan Ai,[a] Chong Zhang,[a] Fu-Min Li,*[b] and Yu Chen*[a]

[a] *Key Laboratory of Macromolecular Science of Shaanxi Province, Key Laboratory of Applied Surface and Colloid Chemistry (Ministry of Education), Shaanxi Key Laboratory for Advanced Energy Devices, School of Materials Science and Engineering, Shaanxi Normal University, Xi'an 710119, PR China. Email: ndchenyu@gmail.com (Y. Chen)*

[b] *School of Chemistry and Chemical Engineering, Huazhong University of Science and Technology, Wuhan 430074, PR China. Email: lifuminxs@gmail.com (F. M. Li)*

Experimental section

Reagents and chemicals

Rhodium (III) 2,4-pentanedionate ($Rh(acac)_3$, ≥97%) was purchased from Shanghai Macklin Biochemical Co., Ltd. (Shanghai, China). Rhodium trichicride ($RhCl_3$ $3H_2O$, ≥99.9%), potassium tetrachloroplatinate (II) (K_2PtCl_4, ≥99.9%) was purchased from Shanghai Jiu Ling chemical Co., Ltd. Polyvinylpyrrolidone (PVP, K30, ≥95%), acetone (C_3H_6O, ≥99.5%), ethanol absolute (C_2H_6O, ≥99.7%), L-Ascorbic acid ($C_6H_8O_6$, ≥99.7%) and formaldehyde aqueous solution (37.0~40.0%) were purchased from Sinopharm Chemical Reagent Co., Ltd. (Shanghai, China). Benzyl alcohol (C_7H_8O, ≥99.0%) was purchased from Guangzhou Jinhuada Chemical Reagent Co., Ltd. All reagents were used as received without further purification.

Synthesis of catalysts

Synthesis of ultrathin Rh metallenes (Rh ML)

$Rh(acac)_3$ (8.0 mg) were dissolved in a mixed solution of benzyl alcohol and formaldehyde (6 mL, $2V_{benzyl\ alcohol} = V_{formaldehyde}$). Using an ultrasound machine for 10 minutes to blend the mixture evenly. It was then transferred to a high-pressure reaction kettle lined with Teflon and kept at 180 °C for 6 hours before being cooled to room temperature.

Synthesis of ultrathin rhodium-platinum bimetallene (RhPt PBML)

K_2PtCl_4 (20 mg) was dissolved in the water (20 mL) and dispersion of Rh NSs (20 mg) into water (60 mL). Mix the two solutions at room temperature and sonicated for 24 h. Then ultrasonic washing and drying.

Synthesis of rhodium-platinum nanodendrites (RhPt NC)

$RhCl_3$ (10.6 mg) and K_2PtCl_4 (2.8 mg) were dissolved in 5 mL of water. Dissolve 70 mg of AA in 1 mL of water. The two were held in a water bath at 80°C for 3 min and mixed well and held for 2.5 h.

Electrochemical measurements

At 30 ± 1°C, the electrochemical analyzer (CHI-660) measures the CV and ampere i-t curves. Based on a three-electrode system, a carbon rod with 5 mm diameter served as an auxiliary electrode, a saturated calomel electrode was used as a reference electrode, and the working electrode was a catalyst-modified glassy carbon. The 10 mg catalyst was dispersed in a mixture of water and isopropanol (5 mL, water: isopropanol = 4:1) to prepare the electrocatalytic ink. The 4 μL catalytic ink was loaded on a glass carbon electrode with a load of 0.114 mg cm^{-2} and dried in a 60°C oven. Coating 3 μL Nafion solution on catalyst surface (0.05 wt%), 60°C drying.

Physical characterization.

Scanning electron microscopy (SEM) measurements are performed on SU-8220 instruments. Transmission electron microscopy (TEM) images and elemental mapping images are tested on JEM-2800 microscopes equipped with dual EDX high flux energy spectroscopy detectors. High-angle annular dark field scanning transmission electron microscopy (HAADF-STEM) was carried out on J Titan Cubed Themis G2 300 (Thermofisher scientific). The powder x-ray diffraction (XRD) results at room temperature were recorded on the SmartLab (9) instrument. Energy dispersion X-ray (EDX) measurements are performed on a quantum 200 instrument. The liquid phase data were tested by Shimazu liquid chromatography. X-ray photoelectron spectroscopy (XPS) data were obtained from an AXIS ULTRA spectrometer (Kratos). inductively coupled plasma atomic emission spectroscopy (ICP-AES) were tested by Avio550.

Calculation formulas.

About Faradaic Efficiency: Faradaic efficiency = (mn*F*)/Q, where F is the Faraday constant, m is moles of products, and n was transferred electrons. For CH_3COOH as product, n is 4, 4 comes from the 4-electron transferring in ethanol oxidation reaction (EOR) C2 pathway. *F* is the faraday constant that equals to 96485 C mol^{-1}. The products concentrations of the electrolyte were investigated by high performance liquid chromatography (HPLC, LC-20AT, Shimadzu). Before testing, adjust pH of electrolyte to 2.5 using sulfuric acid. The concentrations of CH_3COOH were quantified by SPD-20A. Aminex HPX-87H column (Bio-Rad Co., Ltd.) at 30°C was used with 5 mM H_2SO_4 aqueous solution as the eluent. And the Faradaic efficiency of C1 pathway can be calculated by $F_{C1} = 1 - F_{C2}$.

Theoretical section.

In the present study, density functional theory (DFT) calculations were performed using the *Vienna ab initio simulation package* (VASP).[1, 2] The Perdew-Burke Ernzerhof (PBE) exchange correlation functional within the generalized gradient approximation (GGA) was employed,[3] with a 400 eV cutoff for the plane-wave basisset. We constructed 2×2 supercell for Rh, Pt, RhPt model by cleaving the bulk structure along the (111) and (311) direction. Fig. S30-33 shows the details of the calculation model. The Brillouin zones were sampled using a Monkhorst-Packgrid with dimensions of 6 × 6 × 6 and 3 × 3 × 1 for bulk Rh and Pt, (111) and (311) slab models, respectively.[4] The convergence criteria were set at 10^{-4} eV for energy and 0.02 eV $Å^{-1}$for force.[5] To prevent interlayer interactions, a vacuum layer of 15 Å was chosen. During the computational process, full relaxation was performed on all upper half atom layers, while the remaining layers were kept frozen.

The calculation of the EOR process is based on the computational hydrogen electrode (CHE) model proposed by Nørskov. The Gibbs free energy change (ΔG) for each elementary step is determined by the equation 1:

$$\Delta G = \Delta E + \Delta \mathrm{ZPE} - T\Delta S \qquad \text{equation 1}$$

where ΔE represents the total energy obtained from DFT calculations, ΔZPE and ΔS is the zero-point energy and entropy change of intermediate adsorption, respectively. T is the temperature which was set to 298 K.

The d-band center and projected band center (ε_d) can be obtained by equation 2:

$$\varepsilon_d = \frac{\int_{-\infty}^{\infty} n_d(\varepsilon)\varepsilon d_\varepsilon}{\int_{-\infty}^{\infty} n_d(\varepsilon) d_\varepsilon} \qquad \text{equation 2}$$

and d-band width (εw) and d-band filling (Nd) can be obtained by equation 3 and 4:

$$\varepsilon_w = \sqrt{\frac{\int_{-\infty}^{\infty} n_d(\varepsilon)(\varepsilon - \varepsilon_d)^2 d_\varepsilon}{\int_{-\infty}^{\infty} n_d(\varepsilon) d_\varepsilon}} \qquad \text{equation 3}$$

$$N_d = \int_{-\infty}^{0} n_d(\varepsilon) d_\varepsilon \qquad \text{equation 4}$$

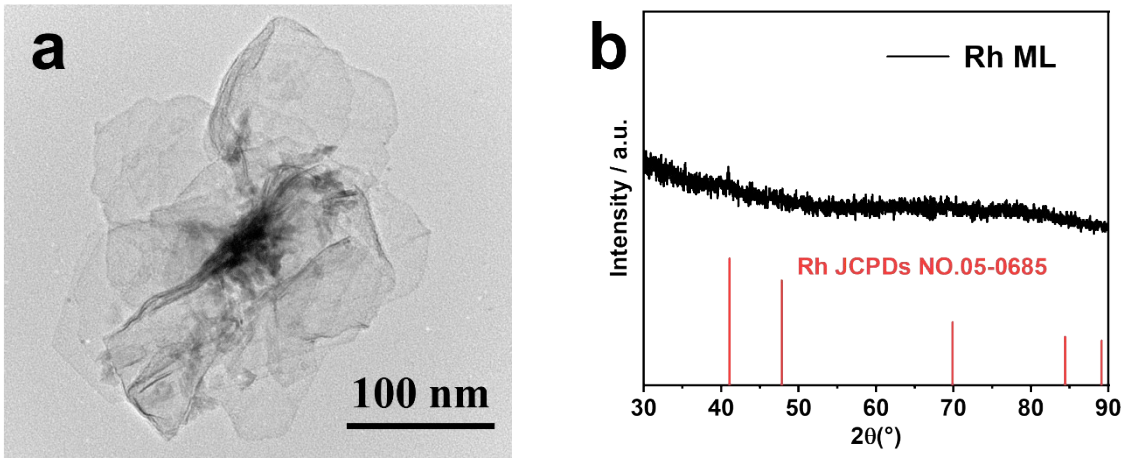

Fig. S1. a) TEM image and b) XRD patterns of Rh ML.

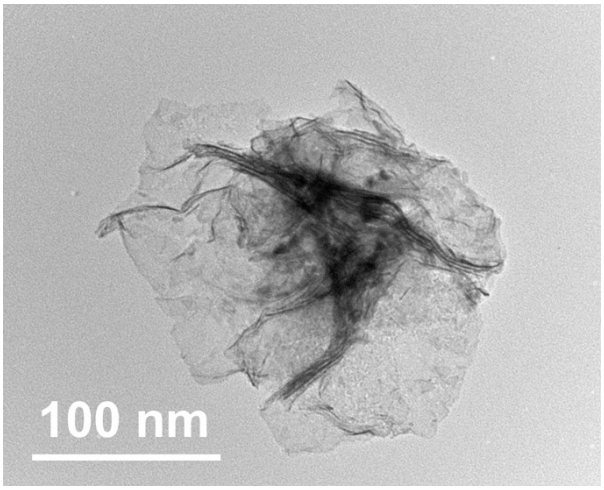

Fig. S2. TEM image of RhPt PBML.

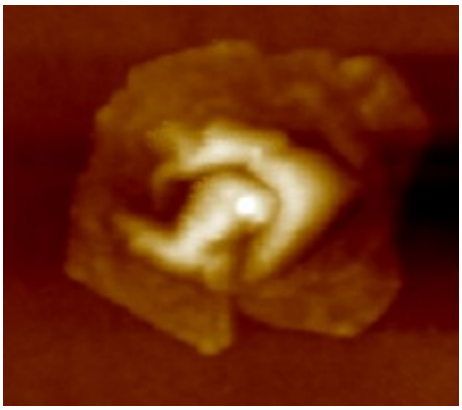

Fig. S3. AFM image of RhPt PBML.

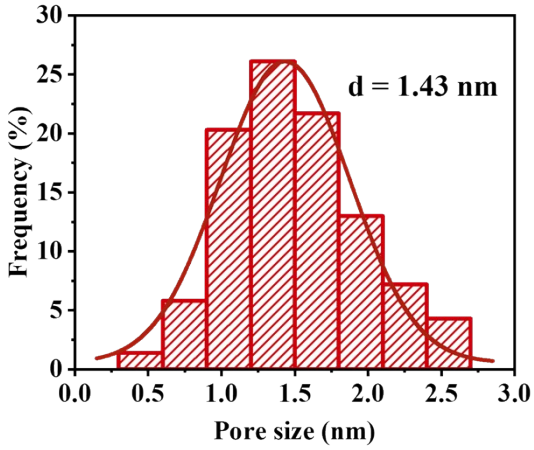

Fig. S4. Pore size distribution histogram of RhPt PBML.

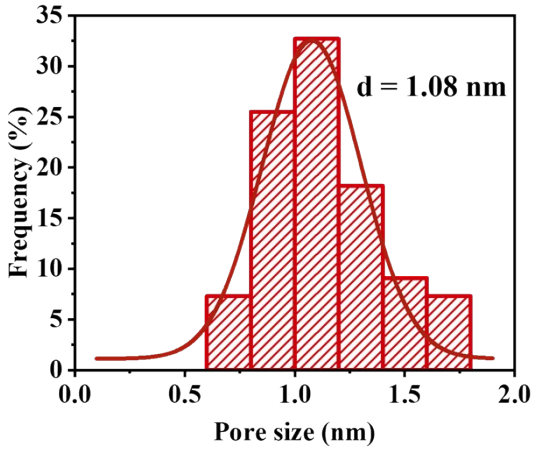

Fig. S5. Nanocrystals size distribution histogram of RhPt PBML.

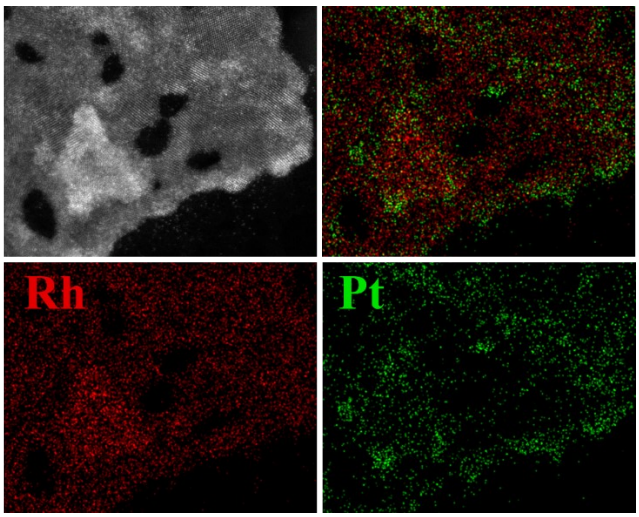

Fig. S6. STEM-EDX elemental mapping images of RhPt PBML.

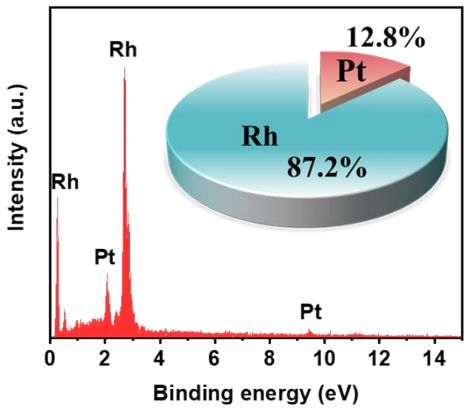

Fig. S7. EDX spectrum of RhPt PBML.

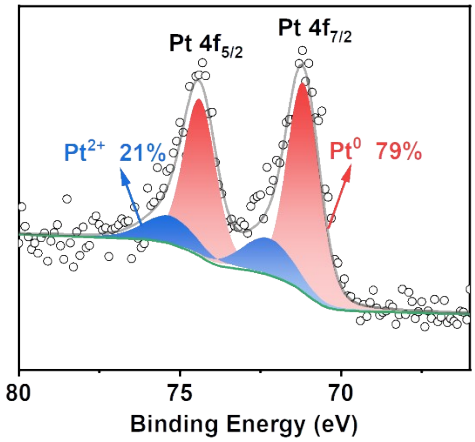

Fig. S8. Pt 4f XPS spectrum of RhPt PBML.

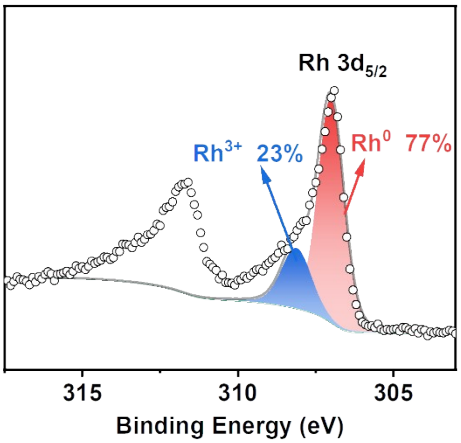

Fig. S9. Rh 3d XPS spectrum of RhPt PBML.

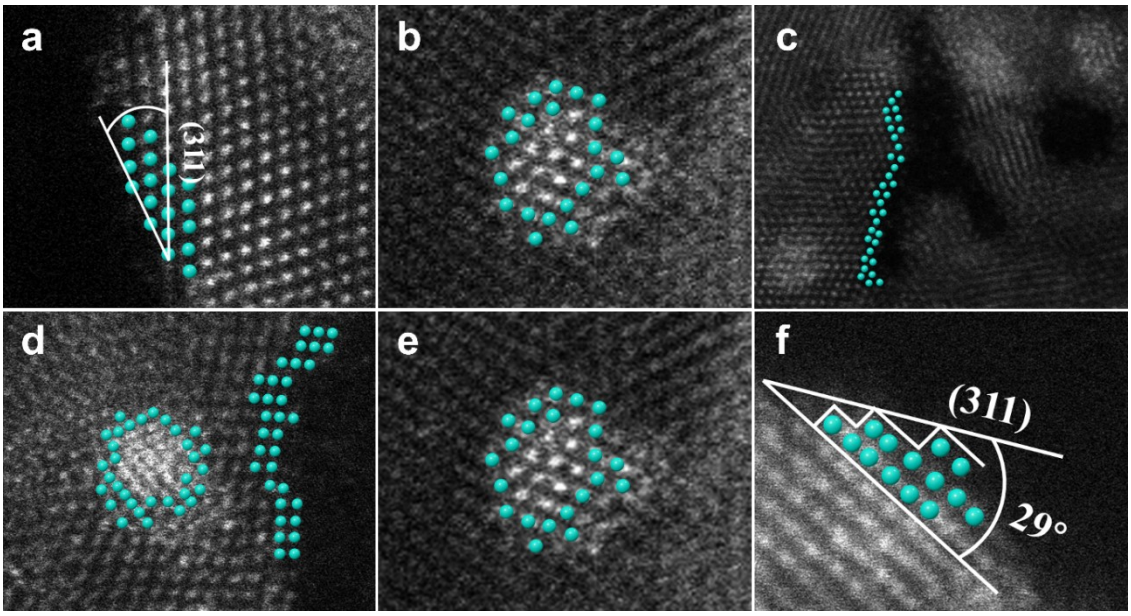

Fig. S10. HAADF-STEM images of RhPt PBML.

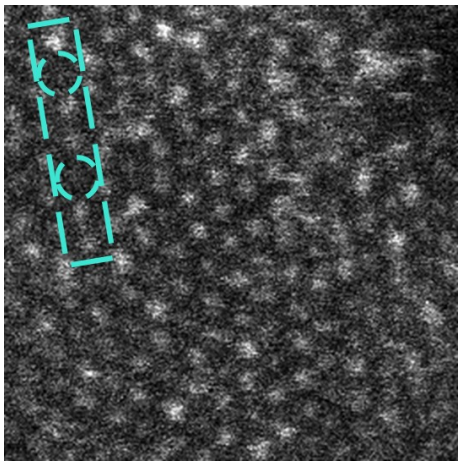

Fig. S11. HAADF-STEM image of RhPt PBML.

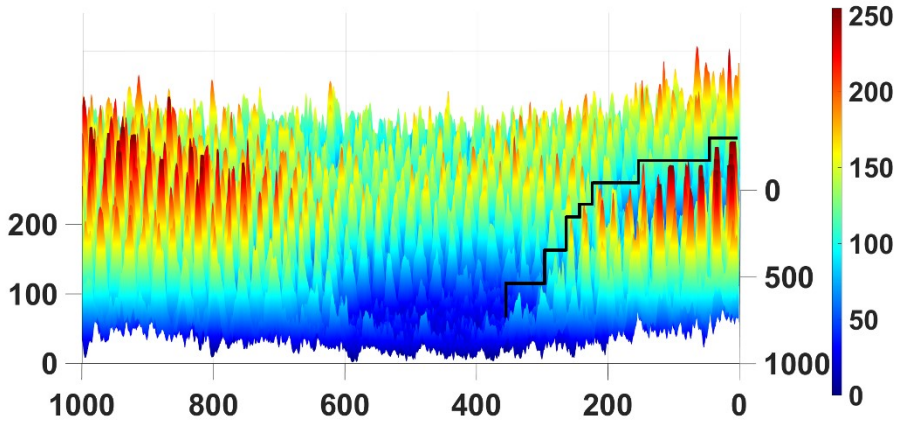

Fig. S12. Corresponding elemental mappings.

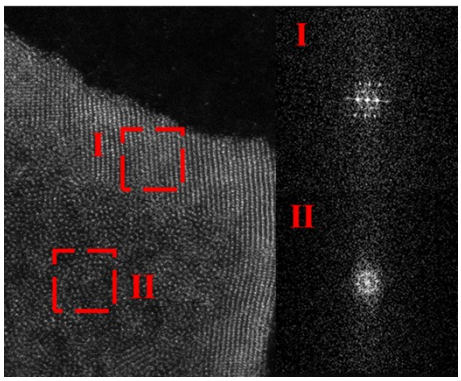

Fig. S13. FFT mode image corresponding to the selected area of Rh ML.

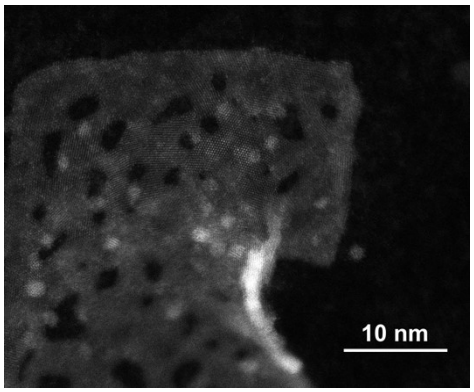

Fig. S14. HAADF-STEM image of RhPt PBML.

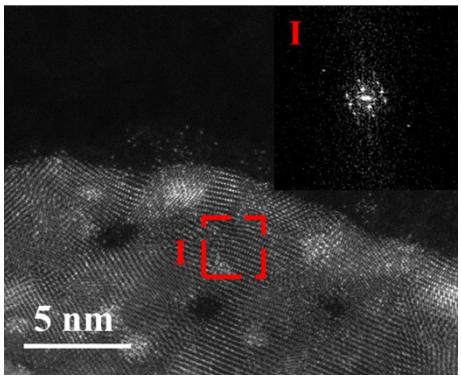

Fig. S15. FFT mode image corresponding to the selected area of RhPt PBML.

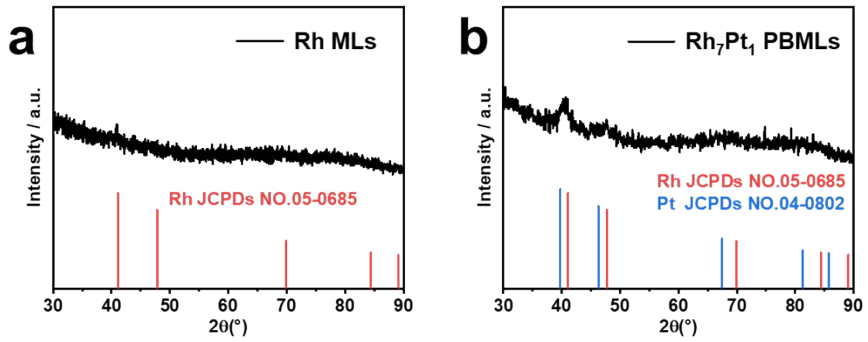

Fig. S16. XRD patterns of a) Rh ML and b) RhPt PBML.

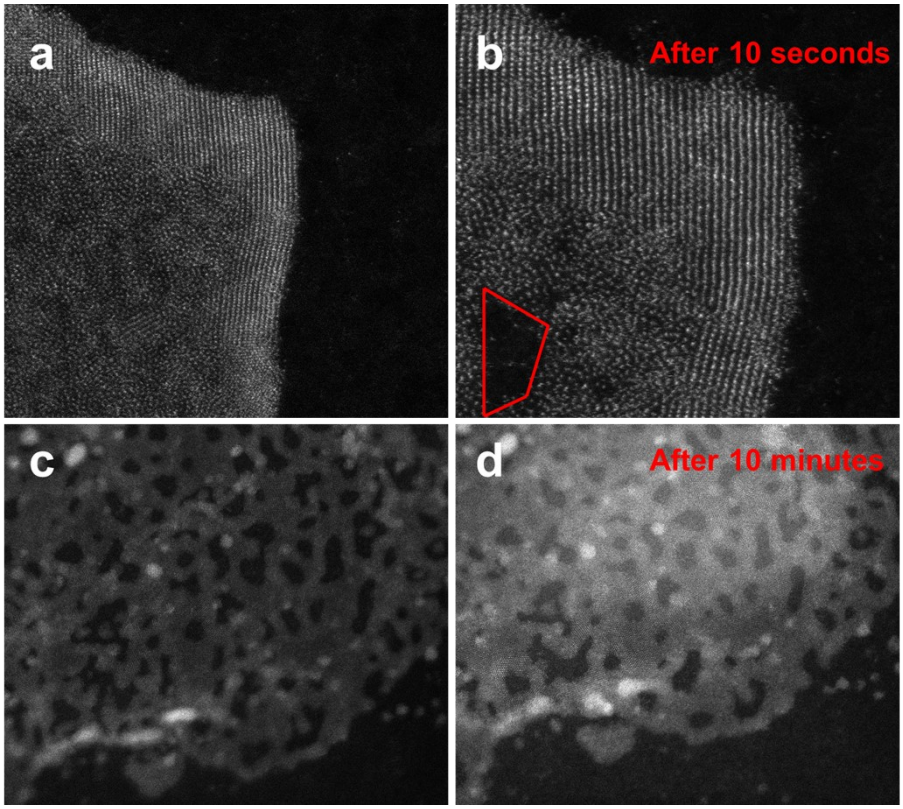

Fig. S17. HADDF-STEM image of Rh MLs (a) before high-intensity electron beam bombardment (b) after 10 seconds high-intensity electron beam bombardment. The HADDF-STEM image of Rh_7Pt_1 MLs (c) before high-intensity electron beam bombardment (d) after 10 minutes high-intensity electron beam bombardment.

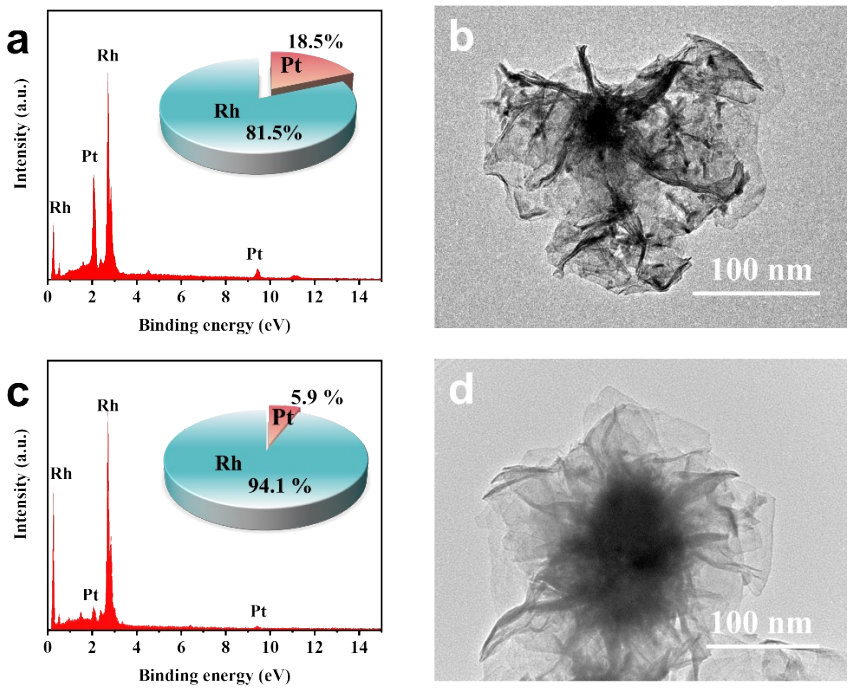

Fig. S18. EDX spectra and TEM images of (a, b) Rh_4Pt_1 PBMLs and (c, d) $Rh_{19}Pt_1$ PBMLs.

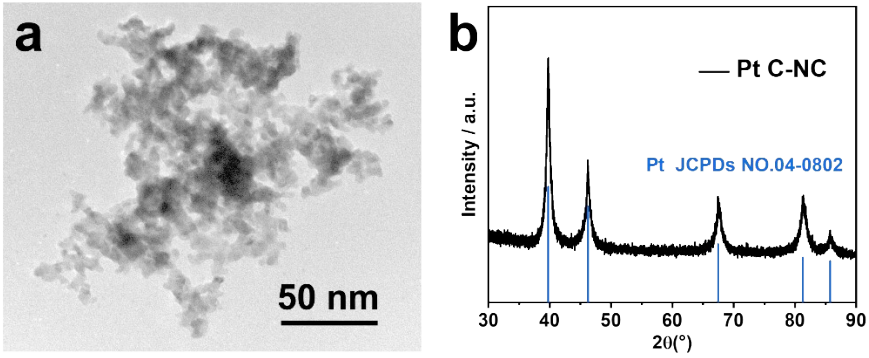

Fig. S19. a) TEM image and b) XRD patterns of Pt C-NC.

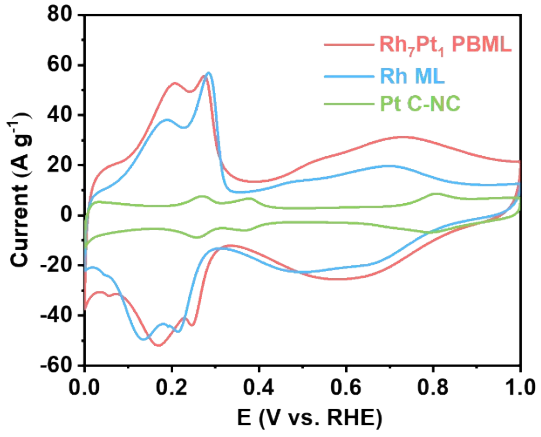

Fig. S20. CV curves of Rh_7Pt_1 PBML, Rh ML and Pt C-NC in N_2-saturated 1 M KOH solution with the scan rate of 0.05 V s^{-1}.

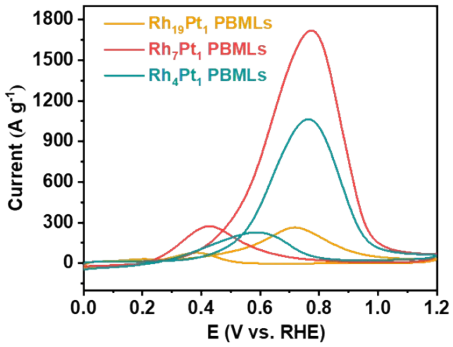

Fig. S21. CV curves of $Rh_{19}Pt_1$ PBMLs, Rh_7Pt_1 PBMLs and Rh_4Pt_1 PBMLs in N_2-saturated 1 M KOH + 1 M CH_3CH_2OH solution with the scan rate of 0.05 V s^{-1}.

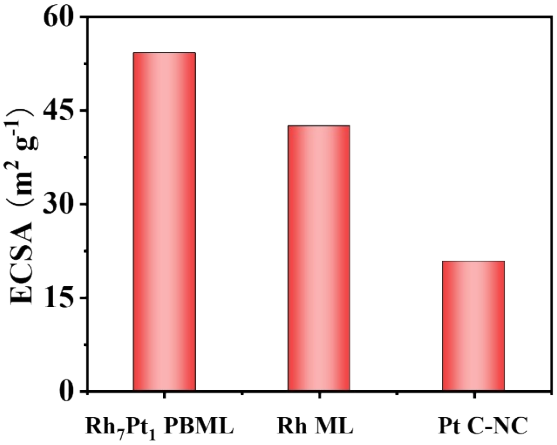

Fig. S22. ECSA of Rh_7Pt_1 PBML, Rh ML and Pt C-NC.

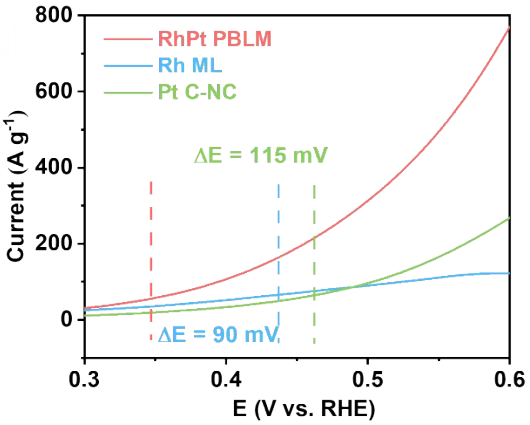

Fig. S23. CV curves of Rh_7Pt_1 PBML, Rh ML and Pt C-NC in N_2-saturated 1 M KOH + 1 M CH_3CH_2OH solution with the scan rate of 0.05 V s^{-1}.

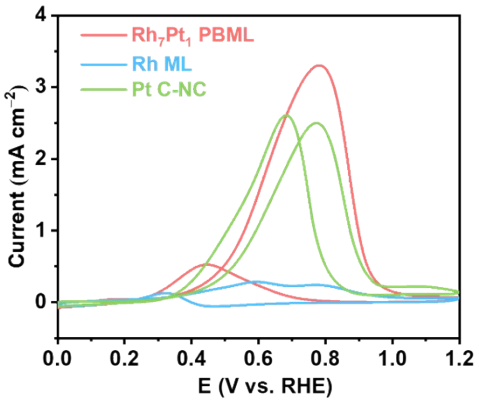

Fig. S24. CV curves of Rh_7Pt_1 PBML, Rh ML and Pt C-NC in N_2-saturated 1 M KOH + 1 M CH_3CH_2OH solution with the scan rate of 0.05 V s^{-1}.

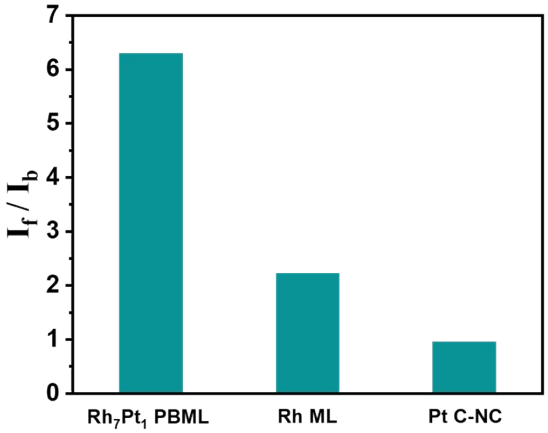

Fig. S25. I_f/I_b values of Rh_7Pt_1 PBML, Rh ML and Pt C-NC.

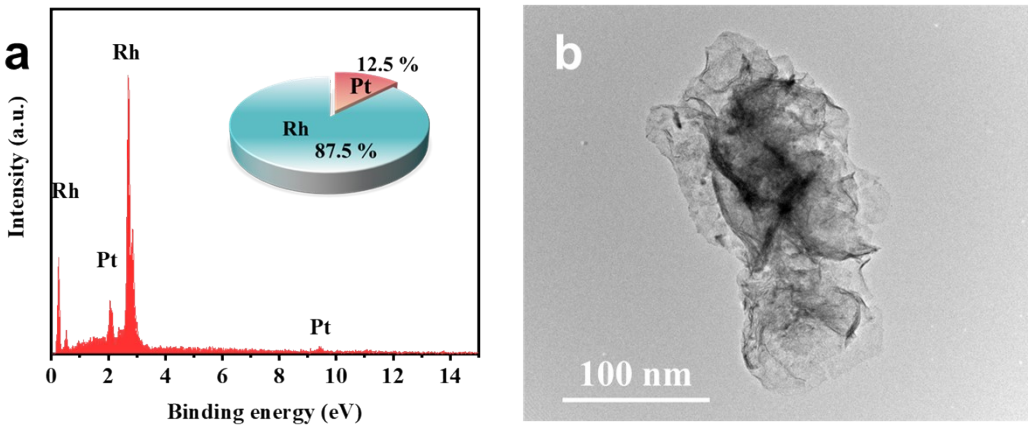

Fig. S26. a) EDX spectrum of Rh_7Pt_1 PBML after the stability test. b) TEM image of Rh_7Pt_1 PBML after the stability test.

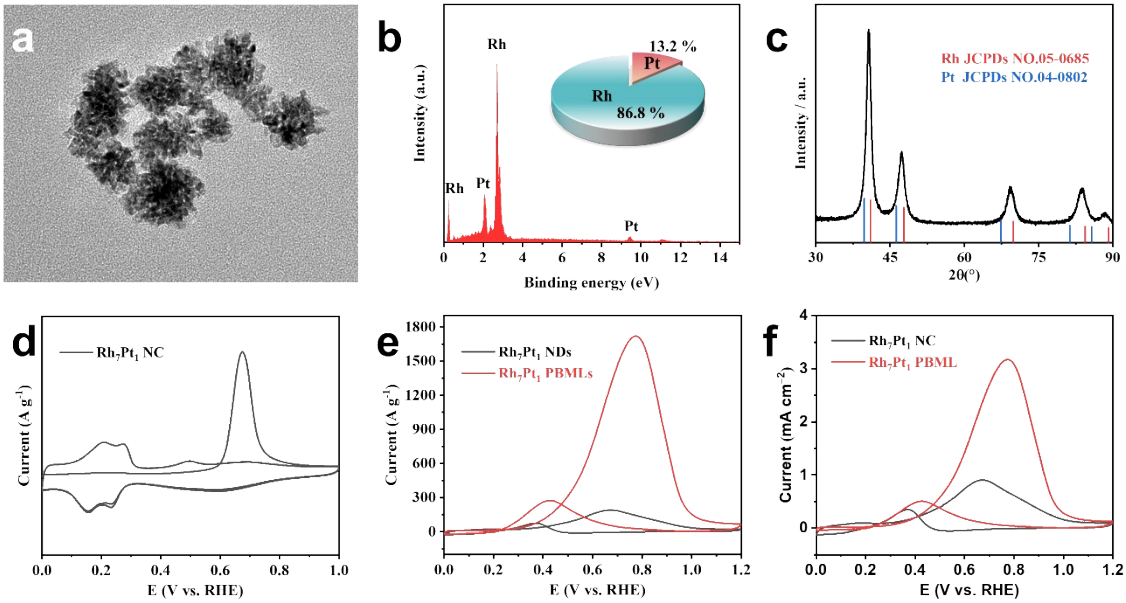

Fig. S27. a) TEM image, b) EDX spectrum and c) XRD of Rh_7Pt_1 NC. d) CO-stripping curves of Rh_7Pt_1 NC. e, f) CV curves of Rh_7Pt_1 PBML and Rh_7Pt_1 NC in N_2-saturated 1 M KOH + 1 M CH_3CH_2OH solution with the scan rate of 0.05 V s^{-1}.

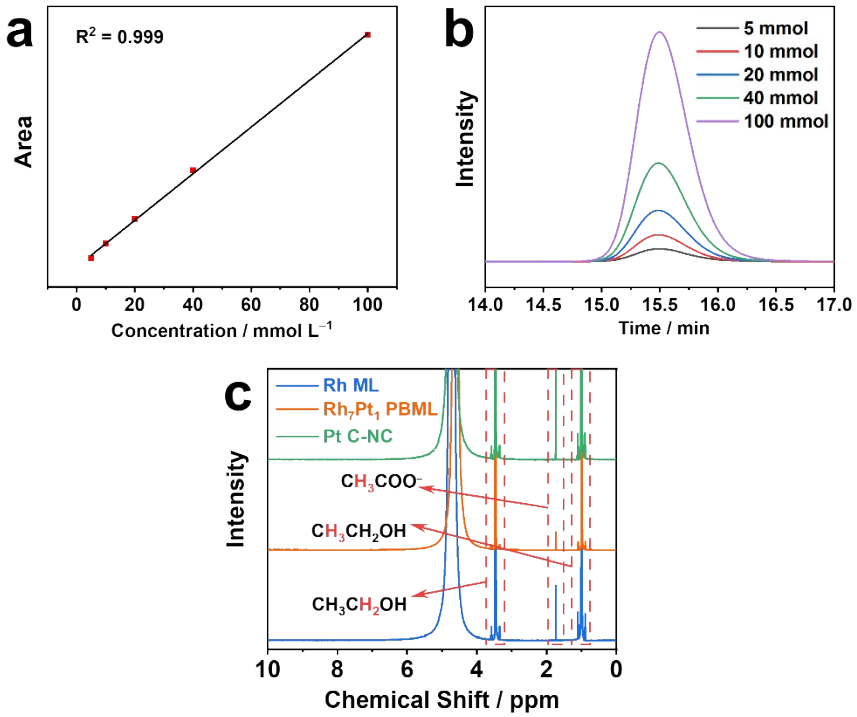

Fig. S28. a) Standard curves and b) test results for different concentrations of acetic acid by HPLC. c) ^1H NMR analysis of the electrolytes after EOR on Rh_7Pt_1 PBML, Pt C-NC and Rh ML. Except for ethanol and water, only acetate was detected.

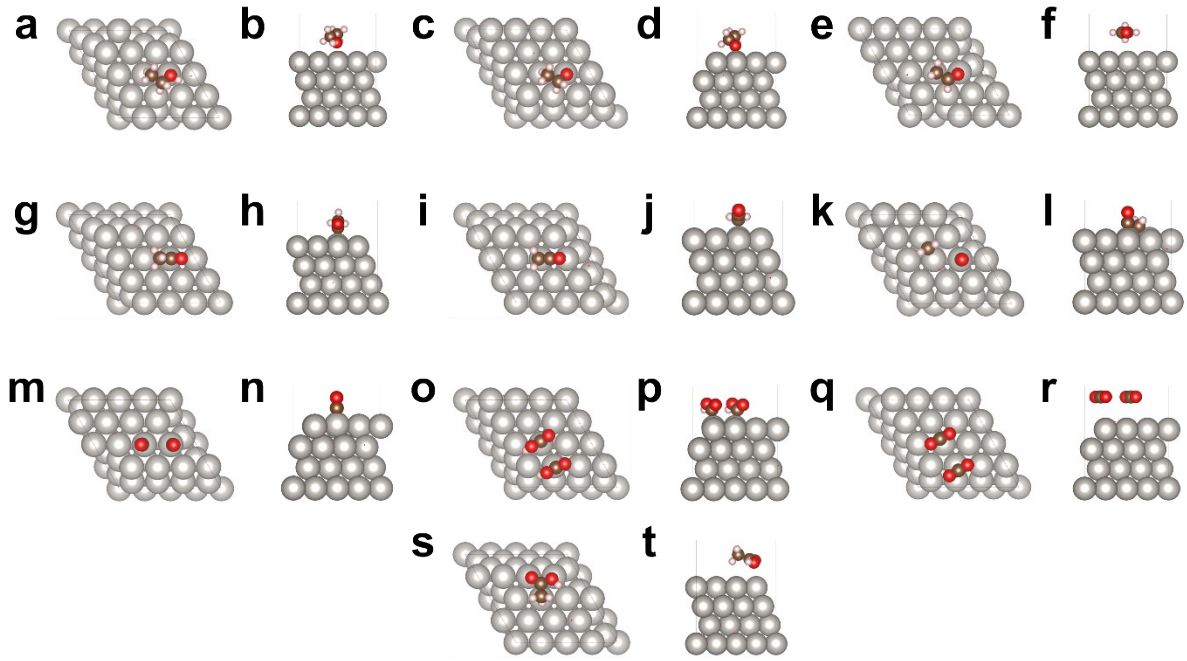

Fig. S29. a, c, e, g, i, k, m, o, q, s) top and b, d, f, h, j, l, n, p, r, t) Side views of $CH_3CH_2OH^*$, $CH_3CH_2O^*$, CH_3CHO^*, CH_3CO^*, CH_2CO^*, $CH_2^* + CO^*$, $2CO^*$, $2COOH^*$, $2CO_2^*$ and CH_3COOH^* on Pt (111) with vertical configuration.

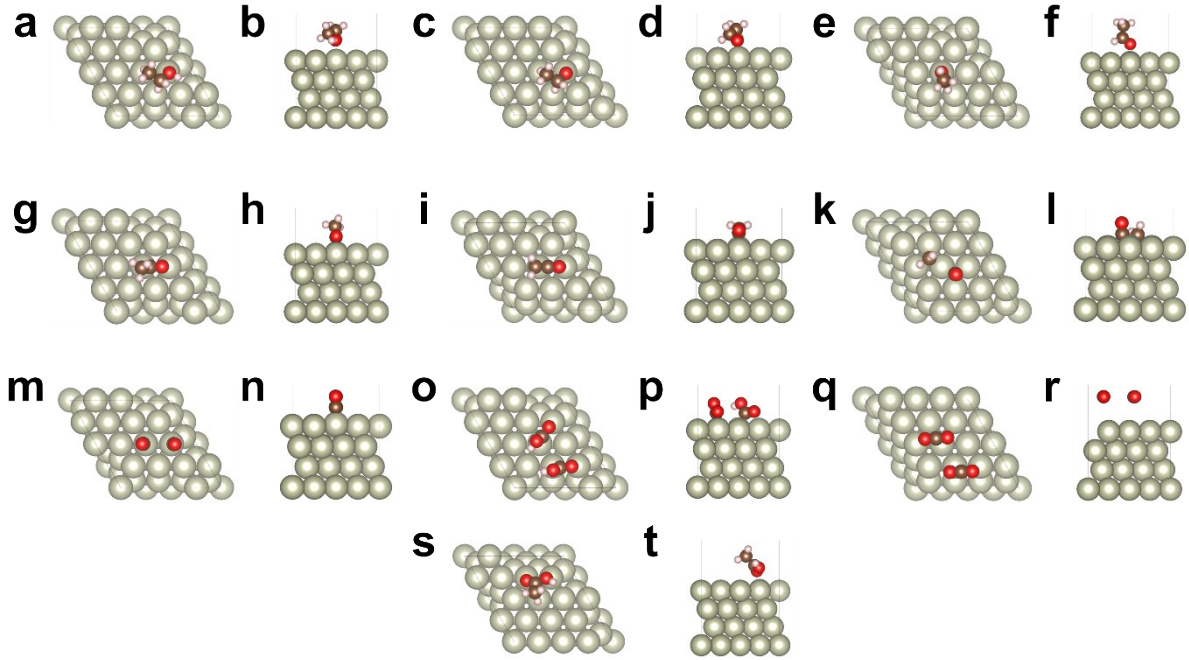

Fig. S30. a, c, e, g, i, k, m, o, q, s) top and b, d, f, h, j, l, n, p, r, t) Side views of $CH_3CH_2OH^*$, $CH_3CH_2O^*$, CH_3CHO^*, CH_3CO^*, CH_2CO^*, $CH_2^* + CO^*$, $2CO^*$, $2COOH^*$, $2CO_2^*$ and CH_3COOH^* on Rh (111) with vertical configuration.

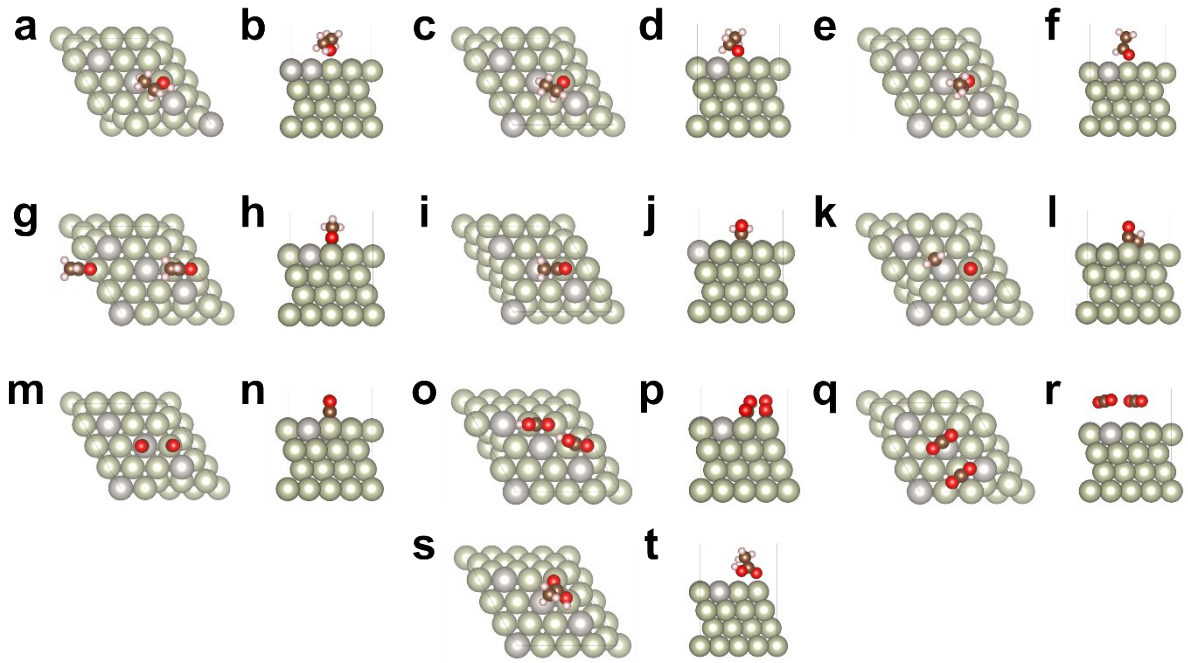

Fig. S31. a, c, e, g, i, k, m, o, q, s) top and b, d, f, h, j, l, n, p, r, t) Side views of $CH_3CH_2OH^*$, $CH_3CH_2O^*$, CH_3CHO^*, CH_3CO^*, CH_2CO^*, $CH_2^* + CO^*$, $2CO^*$, $2COOH^*$, $2CO_2^*$ and CH_3COOH^* on RhPt (111) with vertical configuration.

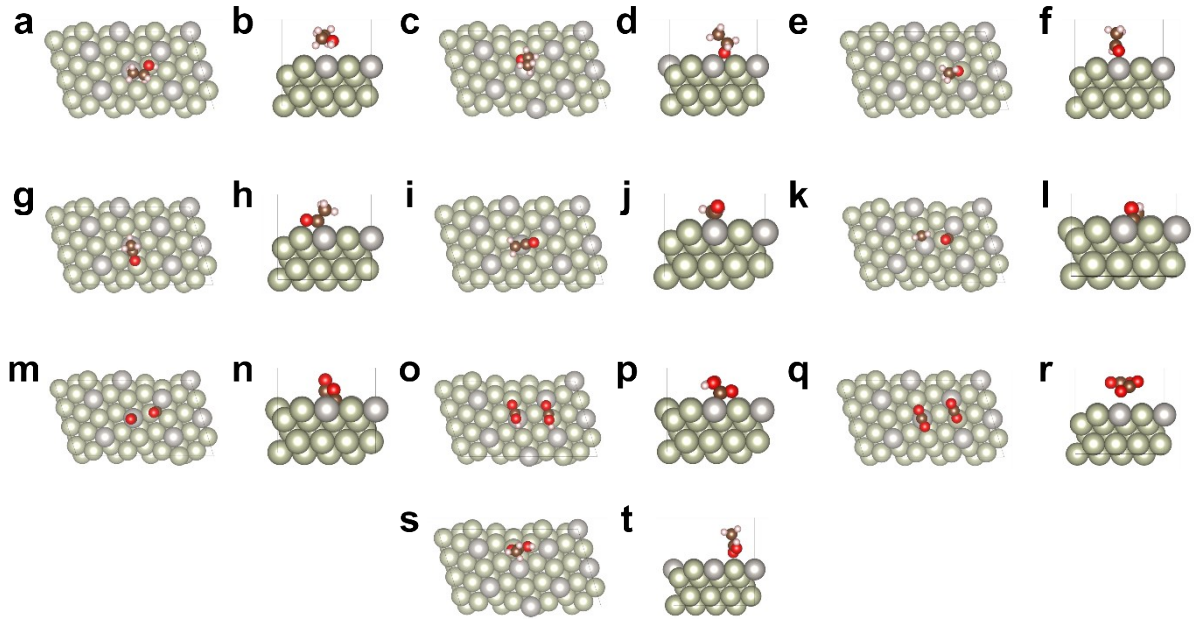

Fig. S32. a, c, e, g, i, k, m, o, q, s) top and b, d, f, h, j, l, n, p, r, t) Side views of $CH_3CH_2OH^*$, $CH_3CH_2O^*$, CH_3CHO^*, CH_3CO^*, CH_2CO^*, $CH_2^* + CO^*$, $2CO^*$, $2COOH^*$, $2CO_2^*$ and CH_3COOH^* on RhPt (311) with vertical configuration.

$$* + CH_3CH_2OH \rightarrow CH_3CH_2OH* \quad (1)$$

$$CH_3CH_2OH* \rightarrow CH_3CH_2O* + H^+ + e^- \quad (2)$$

$$CH_3CH_2O* \rightarrow CH_3CHO* + H^+ + e^- \quad (3)$$

$$CH_3CHO* \rightarrow CH_3CO* + H^+ + e^- \quad (4)$$

$$CH_3CO* \rightarrow CH_2CO* + H^+ + e^- \quad (5)$$

$$CH_2CO* \rightarrow CH_2* + CO* \quad (6)$$

$$CH_2* + CO* + H_2O \rightarrow 2CO* + 4H^+ + 4e^- \quad (7)$$

$$2CO* + 2H_2O \rightarrow 2COOH* + 2H^+ + 2e^- \quad (8)$$

$$2COOH* \rightarrow 2CO_2* + 2H^+ + 2e^- \quad (9)$$

$$2CO_2* \rightarrow 2CO_2 + * \quad (10)$$

Fig. S33. The EOR reaction equations.

Table S1. Atomic ratios of different RhPt PBMLs characterized by EDS and ICP-AES.

Sample	Rh/Pt (At%) from EDX	Rh/Pt (At%) from ICP-AES
Rh_7Pt_1 PBMLs	87.2:12.8	86.9:13.1

Table S2. Advanced catalyst reported in recent years.

No.	Catalysts	Electrolyte	Faradic efficiency (%)	References
	Perforated Rh_7Pt_1 bimetallene (Rh_7Pt_1 PBML)	1M KOH + 1M CH_3CH_2OH @ 60°C	100	**This Work**
	Rh_7Pt_1 PBML	1M KOH + 1M CH_3CH_2OH @ 30°C	85.1	**This Work**
1	PtPb nanosheets (m-PtPb NSs)	1M KOH + 0.1M CH_3CH_2OH	5	[6]
2	$Pt_{0.5}Rh_{0.5}$ hollow sphere (250_$Pt_{0.5}Rh_{0.5}$)	1M KOH + 1M CH_3CH_2OH	38.3	[7]
3	PdCu synthesis of highly curved quasi-single-crystalline mesoporous nanoplates (PdCu SMPs)	1M KOH + 1M CH_3CH_2OH	72.1	[8]
4	Ir-alloyed Pt nanorods (Pt-Ir NRs)	1M KOH + 1M CH_3CH_2OH	61.21	[9]
5	$Pd_3Pt_1Rh_{0.1}$ nanorings	0.1M KOH + 0.5M	45.51	[10]

	($Pd_3Pt_1Rh_{0.1}$ NRs/C)	CH_3CH_2OH		
6	Rh-$Bi(OH)_3$/C	1M NaOH + 1M CH_3CH_2OH	26.2	[11]
7	SnO_2–Rh nanosheets ($0.2SnO_2$-Rh NSs/C)	0.1M KOH + 0.5M CH_3CH_2OH	72.8	[12]
8	Rh is atomically dispersed in a tensile-strained Pt shell on intermetallic PtBi nanoplate (PtBi@$PtRh_1$)	1M KOH + 1M CH_3CH_2OH	24.6	[13]
9	Pd-Au heterophase nanosheet catalyst (Pd-Au HNS/C)	0.1M KOH + 1M CH_3CH_2OH	33.2	[14]
10	Amorphous PtO_x interface on Pt/WO_3 nanosheets (Pt/α-PtO_x/WO_3)	0.1M NaOH + 0.5M CH_3CH_2OH	21.9	[15]

Table S3. Summary of vibration bands of the in situ FTIR specturm

Band frequency (cm^{-1})	Assignment	References
2029 – 2121	$\nu(CO_L)$	[16-20]
1886 – 1967	$\nu(CO_B) + \nu(CO_M)$	[16-20]
~ 1662	double bonded CO_{ad}	[21-23]
~ 1620	ν(C=O) of adsorbed acetyl	[20-22, 24]
~ 1530	ν_{as}(OCO) of solution acetate	[25, 26]
~ 1423	ν_s(OCO) of bridge-bonded acetate	[25, 26]
~ 1408	CO_3^{2-}	[26-28]
~ 1358	Glycolat, HCO_3^-	[21, 27, 29]

Table S4. The d-band center, d-band filling and d-band width of Rh (111), Pt (111), RhPt (111) and RhPt (311).

	d-band center (eV)	d-band filling (per atom)	d-band width (eV)
Rh (111)	-1.71	6.77	2.28
Pt (111)	-2.27	7.89	2.21
RhPt (111)	-1.76	6.77	2.29
RhPt (311)	-1.68	7.01	2.09

Notes and references

1 G. Kress and J. Furthmüller, *Comput. Mater. Sci*, 1996, **6**, 15.
2 G. Kress and J. Furthmüller, *Phys. Rev. B*, 1996, **54**, 11169.
3 J. P. Perdew, K. Burke and M. Ernzerhof, *Phys. Rev. Lett.*, 1996, **77**, 3865.
4 H. J. Monkhorst and J. D. Pack, *Phys. Rev. B*, 1976, **13**, 5188.
5 P. E. Blochl, *Phys. Rev. B*, 1994, **50**, 17953.

6 W. Ao, H. Ren, C. Cheng, Z. Fan, P. Yin, Q. Qin, Q. Zhang and L. Dai, *Angew. Chem. Int. Ed.*, 2023, **24**, e202305158.
7 K. H. Kim, G. M. Hobold, K. J. Steinberg and B. M. Gallant, *ACS Nano*, 2023, **17**, 14176.
8 H. Lv, L. Z. Sun, Y. Z. Wang, S. H. Liu and B. Liu, *Adv. Mater.*, 2022, **34**, 2203612.
9 Y. Fang, S. Guo, D. Cao, G. Zhang, Q. Wang, Y. Chen, P. Cui, S. Cheng and W. Zuo, *Nano Res.*, 2022, **15**, 3933.
10 H. Tian, R. Zhu, P. Deng, J. Li, W. Huang, Q. Chen, Y. Q. Su, C. Jia, Z. Liu, Y. Shen and X. Tian, *Small*, 2022, **18**, e2203506.
11 B. Lan, Q.-L. Wang, Z.-X. Ma, Y.-J. Wu, X.-L. Jiang, W.-S. Jia, C.-X. Zhou and Y.-Y. Yang, *Appl. Catal. B*, 2022, **300**, 120728.
12 S. X. Bai, Y. Xu, K. L. Cao and X. Q. Huang, *Adv. Mater.*, 2021, **33**, 2005767.
13 S. Luo, L. Zhang, Y. Liao, L. Li, Q. Yang, X. Wu, X. Wu, D. He, C. He, W. Chen, Q. Wu, M. Li, E. J. M. Hensen and Z. Quan, *Adv. Mater.*, 2021, **33**, 2008508.
14 F. Lv, W. Zhang, M. Sun, F. Lin, T. Wu, P. Zhou, W. Yang, P. Gao, B. Huang and S. Guo, *Adv. Energy Mater.*, 2021, **11**, 2100187.
15 L. Xiao, G. Li, Z. Yang, K. Chen, R. Zhou, H. Liao, Q. Xu and J. Xu, *Adv. Funct. Mater.*, 2021, **31**, 2100982.
16 C. Zhu, B. Lan, R.-L. Wei, C.-N. Wang and Y.-Y. Yang, *ACS Catal.*, 2019, **9**, 4046.
17 M. Li, Z. Zhao, W. Zhang, M. Luo, L. Tao, Y. Sun, Z. Xia, Y. Chao, K. Yin, Q. Zhang, L. Gu, W. Yang, Y. Yu, G. Lu and S. Guo, *Adv. Mater.*, 2021, **33**, 2103762.
18 A. Cuesta, A. Couto, A. Rincón, M. C. Pérez, A. López-Cudero and C. Gutiérrez, *J. Electroanal. Chem.*, 2006, **586**, 184.
19 Y.-G. Yan, Y.-Y. Yang, B. Peng, S. Malkhandi, A. Bund, U. Stimming and W.-B. Cai, *J. Phys. Chem. C*, 2011, **115**, 16378.
20 W. Yan, G. Li, S. Cui, G. S. Park, R. Oh, W. Chen, X. Cheng, J. M. Zhang, W. Li, L. F. Ji, O. Akdim, X. Huang, H. Lin, J. Yang, Y. X. Jiang and S. G. Sun, *J. Am. Chem. Soc.*, 2023, **145**, 17220.
21 Y. Wang, M. Zheng, Y. Li, C. Ye, J. Chen, J. Ye, Q. Zhang, J. Li, Z. Zhou, X. Z. Fu, J. Wang, S. G. Sun and D. Wang, *Angew. Chem. Int. Ed.*, 2022, **61**, e202115735.
22 M. Heinen, Z. Jusys and R. J. Behm, *J. Phys. Chem. C*, 2010, **114**, 9850.
23 Q. Chang, Y. Hong, H. J. Lee, J. H. Lee, D. Ologunagba, Z. Liang, J. Kim, M. J. Kim, J. W. Hong, L. Song, S. Kattel, Z. Chen, J. G. Chen and S. I. Choi, *Proc. Natl. Acad. Sci. U.S.A.*, 2022, **119**, e2112109119.
24 Y.-Y. Yang, J. Ren, Q.-X. Li, Z.-Y. Zhou, S.-G. Sun and W.-B. Cai, *ACS Catal.*, 2014, **4**, 798.
25 K. Wei, H. Lin, X. Zhao, Z. Zhao, N. Marinkovic, M. Morales, Z. Huang, L. Perlmutter, H. Guan, C. Harris, M. Chi, G. Lu, K. Sasaki and S. Sun, *J. Am. Chem. Soc.*, 2023, **145**, 19076.
26 J. Zhang, J. Ye, Q. Fan, Y. Jiang, Y. Zhu, H. Li, Z. Cao, Q. Kuang, J. Cheng, J. Zheng and Z. Xie, *J. Am. Chem. Soc.*, 2018, **140**, 11232.
27 X. Yang, K. X. Yao, J. Y. Ye, Q. Yuan, F. Zhao, Y. Li and Z. Zhou, *Adv. Funct. Mater.*, 2021, **31**, 2103671.
28 P. A. Christensen and A. Hamnett, *J. Electroanal. Chem.*, 1989, **260**, 347.
29 H. Wang, B. Jiang, T.-T. Zhao, K. Jiang, Y.-Y. Yang, J. Zhang, Z. Xie and W.-B. Cai, *ACS Catal.*, 2017, **7**, 2033.